The gravitationally consistent sea–level fingerprint of future terrestrial ice loss

G. Spada

Dipartimento di Scienze di Base e Fondamenti (DiSBeF), Università di Urbino "Carlo Bo", Urbino, Italy

J. L. Bamber and R. T. W. L. Hurkmans

Bristol Glaciology Centre, University of Bristol, UK

G. Spada, Dipartimento di Scienze di Base e Fondamenti (DiSBeF), Università di Urbino "Carlo Bo", Urbino, Italy (Email: giorgio.spada@gmail.com).

J. Bamber and R. Hurkmans, Bristol Glaciology Centre, University of Bristol, UK.

We solve the sea–level equation to investigate the pattern of the gravitationally self–consistent sea–level variations (fingerprints) corresponding to modeled scenarios of future terrestrial ice melt. These were obtained from separate ice dynamics and surface mass balance models for the Greenland and Antarctic ice sheets and by a regionalized mass balance model for glaciers and ice caps. For our mid–range scenario, the ice melt component of total sea–level change attains its largest amplitude in the equatorial oceans, where we predict a cumulative sea–level rise of ~ 25 cm and rates of change close to 3 mm/yr from ice melt alone by 2100. According to our modeling, in low–elevation densely populated coastal zones, the gravitationally consistent sea–level variations due to continental ice loss will range between 60 and 144 % of the global mean. This includes the effects of glacial–isostatic adjustment, which mostly contributes across the lateral forebulge regions in North America. While the mid range ocean–averaged elastic–gravitational sea–level variations compare with those associated with thermal expansion and ocean circulation, their combination shows a complex regional pattern, where the former component dominates in the Equatorial Pacific Ocean and the latter in the Arctic Ocean.

1. Introduction

The non–uniform effect of terrestrial ice melt (TIM) on relative sea level (RSL) was recognised over a century ago [Woodward, 1888]. The modern theory [Farrell and Clark, 1976] has been further developed more recently to include, for example, changes in Earth rotation and shoreline migration [Milne and Mitrovica, 1998] and is generally termed the sea level equation (SLE). This equation has been used to investigate the impact of idealised melt scenarios for Greenland and Antarctica [Mitrovica *et al.*, 2001] and to examine the RSL pattern resulting from observed recent TIM [Bamber and Riva, 2010]. This latter study found that maxima occurred at low latitudes, in the Western Pacific in particular, and had a marked zonal gradient driven, primarily, by the dominant sources in both polar regions. To date, however, the SLE has not been used to examine the RSL pattern resulting from prognostic predictions of future land ice melting, nor to examine the relative importance of TIM and steric effects regionally.

Here, we combine predictions from numerical models for the evolution of the Greenland (GrIS) and Antarctic (AIS) ice sheets with a regionalized model for glaciers and ice caps to investigate the gravitationally consistent signature of future TIM based on the A1B SRES scenario and the ECHAM–5 GCM [Meehl *et al.*, 2007]. Steric and ocean dynamic processes are also non–uniformly distributed and we examine the relative importance of these with respect to TIM, using the same GCM and greenhouse gas forcing.

2. Data processing and methods

For the Greenland and Antarctic ice sheets, volume changes are caused by both ice dynamics and surface mass balance (SMB). SMB is driven by accumulation and surface melting in Greenland and just the former in Antarctica. These fields were obtained from two regional climate models (RCMs): MAR for Greeenland [Fettweis *et al.*, 2007] and RACMO for Antarctica [Lenaerts *et al.*, 2012]. Both were forced by the ECHAM5 GCM under scenario A1–B. Annual SMB anomalies were calculated with respect to the baseline period 1989–2008, and regridded to a spatial resolution of 1°. The period 1992–2000 was appended to the scenarios using re-analysis data (ERA-Interim for Greenland, ERA–40 for Antarctica) and downscaled using the same RCMs. Ice dynamics, represented as grounding line flux anomalies with respect to a reference year, were taken from ice sheet model simulations forced by the same RCMs. SMB and ice dynamics sources are shown in Fig. 1. F1

For Antarctica, from an ensemble of 81 model runs, two simulations were selected: a "mid–range" (MR) scenario contributing $\sim$ 7 cm of mean sea–level rise (SLR) by 2100, and a "high–end" (HE) scenario contributing $\sim$ 30 cm. Only volume changes of ice above floatation (i.e. contributing to SLR) are taken into account here. Antarctica is divided into 15 major drainage basins, and in each basin the volume change is evenly distributed over all 1° grid cells with an average velocity Rignot *et al.* [2011a] over 50 m yr^{-1}. For Greenland, flow-line model simulations were carried out for three outlet glaciers: Jakobshavn isbræ, Petermann and Helheim glaciers and upscaled to obtain total volume changes due to calving for three sectors of the GrIS following a previous approach [Price *et al.*, 2011]. For the MR scenario the model was calibrated against present–day observations. To obtain the HE scenario, the bedrock data, an important source of uncertainty, was perturbed by its two-sigma error estimate and perturbed model parameters were prescribed.

Within each sector, volume changes are distributed evenly over all grid cells with average velocity [Moon *et al.*, 2012] over 100 m yr^{-1}. We assume the ice sheets were close to balance until about 1992 [Rignot *et al.*, 2011b], when we prescribe the calving flux anomalies to be zero, and interpolate linearly between 1992 and the initial scenario values in 2001. For Greenland, volume changes in the MR and HE scenarios contribute ~ 4 and ~ 6 cm SLR by 2100, respectively.

Volume changes for glaciers and ice caps (GIC) (Fig. 1c) are derived from a regionalized glacier mass balance model that uses temperature and precipitation anomalies for 19 glacierized sectors globally. The same GCM forcing was used as for the ice sheets and steric response. The sensitivities of the regional glacier responses were calibrated using automatic weather station data for 80 benchmark glaciers [Giesen and Oerlemans, 2012]. As for Greenland, for the MR and HE scenarios, a calibrated version and a version with perturbed parameters were used, respectively. For peripheral GIC around the ice sheets, we used the GIC results solely and masked out overlapping ice sheet model regions.

Using the Fortran code SELEN [Spada and Stocchi, 2007], the SLE is solved in two steps. In the first step, we only account for the ice sources described in Fig. 1 and we assume an elastic rheology (the time scale is small compared with the Maxwell mantle relaxation time). The time series shown in Fig. 1 were smoothed by a 10–year running average for each grid cell, integrated in time, and converted to decadally averaged volumes. In the second step, we account for the effects of the glacio–isostatic adjustment (GIA) of the Earth to the melting of late–Pleistocene ice sheets. Here the SLE is solved using a Maxwell visco–elastic rheology and employing, in particular, model ICE–5G(VM2) [Peltier, 2004].

In the short time window considered, the GIA component evolves at a constant rate. In both steps, we solve the SLE iteratively to a maximum harmonic degree 128 by the pseudo–spectral method, including rotational effects on sea–level change [Milne and Mitrovica, 1998]. In all simulations, the solution of the SLE is expressed in terms of RSL. The variation of "absolute" sea–level, which would be observed by satellite altimetry, is $RSL + U$, where U is vertical displacement of the solid surface of the Earth.

3. Results

Fig. 2 shows the TIM component of RSL expected for the year 2100, relative to 1992, F2 for the MR (a) and HE (b) scenarios (see Fig. 1). The maps show a somewhat complex pattern but they clearly indicate that a SLR is expected almost everywhere, except in the near field of areas of large TIM: predominantly Greenland and West Antarctica. The geometry of the RSL variation is a consequence of the elastic regional uplift caused by ice un–loading and the decreased gravitational force between the depleting ice and the surrounding ocean. With increasing distance, the amplitude of vertical deformation decreases and SLR dominates the global pattern, reaching values in excess of the eustatic amplitude generally at latitudes below about 30° (the eustatic SLR represents the spatially uniform response for a rigid, non–self–gravitating Earth, and is obtained by ocean–averaging the fingerprints). The RSL patterns in Fig. 2 qualitatively agree with Mitrovica *et al.* [2001], who considered sea–level fingerprints corresponding to geometrically simple, idealised ice sources. The global pattern is, however, fairly insensitive to the localised distribution of ice loss except in the near field of the sources [Bamber and Riva, 2010; Spada *et al.*, 2012].

The dominant localised sources of loss in both scenarios are West Antarctic calving and the GrIS (Fig. 1). Although the integrated GIC response is similar in magnitude to the AIS and larger than the GrIS, it is spread over a large part of the Earth's surface and has, therefore, a smaller localised effect on RSL. This explains, in Fig. 2, the large sea–level fall predicted off the Antarctic Peninsula, which, according to our computations, will be subject to uplift rates as large as ~ 5 mm/yr in response to ice un–loading, and in the region surrounding Greenland and the Svalbard archipelago. The sea–level fingerprints of Fig. 2 are characterized by a distinct zonal pattern with a strong equatorial symmetry, which reflects the dipole pattern of the major concentrations of TIM in Fig. 1. For both scenarios, the largest increases are expected in the equatorial oceans where SLR exceeds the eustatic value shown by green contours. In these regions the maxima are around 25% greater than eustatic. This RSL pattern is broadly similar to the present-day fingerprint due to TIM [Bamber and Riva, 2010].

Maps of the rates of sea–level variation expected for the year 2100, shown in Fig. S1, FS1
have a similar pattern to the cumulative RSL of Fig. 2. At this epoch, maximum values of ~ 3 and ~ 8 mm/yr are predicted at equatorial latitudes for the MR and HE scenarios, respectively, in the same regions that experience the maximum amount of cumulative sea–level (Fig. 2). However, according to our projections in Fig. 1, rates of this amplitude can be considered as representative only of the second half of the 21st Century, at which point there is an acceleration in ice loss from both the AIS and GIC (during previous decades, these rates should be reduced by a factor of ~ 2). The spatially averaged rate of sea–level rise for the MR scenario is ~ 3 mm/yr (not including steric effects). The TIM

rates significantly exceed the (GIA–corrected) instrumental observations of SLR since 1880 (1.8 ± 0.1 mm/yr) [Douglas, 1997].

A cursory inspection of Fig. 2 indicates that the cumulative RSL along European coastlines does not exceed the eustatic value (this is also observed for the trends in Fig. S1). This results specifically from mass loss from the GrIS and other Arctic GICs. However, the rate is close to eustatic in north America, and largely above in Southeast Asia and Africa. In Fig. S2 we consider RSL projections at specific locations of interest along the coastlines (tide gauges and cities in low–elevation coastal zones). FS2

4. Discussion and conclusions

Here, the focus has been on the gravitatonally consistent fingerprint of future terrestrial ice loss. For the melting scenarios used, the patterns of SLR are fixed and will only change significantly if the relative contributions of the AIS and Arctic ice masses change significantly. The pattern is a consequence of localised elastic uplift and changes to the geoid as a consequence of mass redistribution. Thermal expansion and ocean circulation also have a non–uniform impact on the pattern of SLR [Yin *et al.*, 2010]. For convenience, we will refer to these as the ocean response. It is, therefore, interesting to consider the relative importance of oceanic and TIM effects on the future pattern of SLR and to see where these effects may be compounded or possibly compensating. Slangen *et al.* [2012] combined GCM model ensemble oceanic and TIM signatures using data from the IPCC AR4 simulations but with a crude estimate of future TIM, resulting in the ocean response being the main source of SLR. As is the case here, their TIM fluxes were not coupled to the AOGCM simulations.

Here, we use the ocean response signal from the ECHAM–5 A1–B simulation [Meehl *et al.*, 2007] for consistency with the TIM forcing but it should be noted that this was not done in a coupled experiment, which is beyond the scope of this study. Thus, the ocean response is consistent with the greenhouse gas forcings used but not with the TIM fluxes produced by the offline ice sheet and glacier models. For the HE scenario, in particular, the ocean response would likely be significantly altered by our TIM fluxes in a fully coupled experiment. For our MR scenario, the eustatic TIM contribution is 24 cm in terms of RSL, which is a similar magnitude to the ocean response for ECHAM–5 A1B of 27 cm [Meehl *et al.*, 2007]. For the HE scenario, the TIM contribution is 61 cm, which is $\sim$ double the ocean signal. Thus in the MR case there will be areas where the ocean response is larger than TIM and vice versa but not for the HE scenario. The TIM and ocean fingerprints are shown in Figs. 3 and 4, showing the total (TIM+ocean) contribution and the fraction of the total SLR due to TIM for both scenarios, respectively. Here, the TIM contribution is expressed in terms of RSL and does not include the GIA component of sea–level change since its importance is limited to formerly glaciated areas and is not an important fraction of the total SLR, even in the MR scenario (see Fig. S2). In Fig. 4, a fraction greater than 0.5 indicates that TIM is larger than the ocean response and vice versa. F 3 F 4

From the results in Figs. 3 and 4, it is apparent that the Southern Ocean is dominated by the TIM signal, even for the MR scenario because the ocean response is significantly below the global mean but this is also an area where TIM is less than eustatic (Fig. 2) and thus a region that experiences considerably less than the mean total SLR response of 48 cm (i.e. TIM plus ocean response, see Fig. 3). Across a large swathe of the Southern

Ocean total SLR is close to zero and, in the vicinity of the Antarctic Peninsula, and West Antarctica negative. Conversely the Arctic Ocean is a region where the ocean response is greater than the global mean while TIM is less (Fig. 2). For the MR scenario this results in a total SLR that is close to the global mean, except for the Chukchi Sea where it reaches almost a factor two more at about 80 cm (Fig. 3). TIM dominates SLR across the Equatorial Pacific Ocean and into a large part of the Indian Ocean, which are all areas where the ocean response is close to, or less than, the global mean. The other region where TIM dominates for the MR scenario is in the vicinity of the Kuroshio Current. For the HE scenario, TIM is dominant everwhere except for a region around the Antarctic Peninsula, West Antarctica and, surprisingly, the Arctic Ocean again. For reasons discussed above, this conclusion is, however, tentative and should be confirmed using a coupled AOGCM forced with the TIM fluxes used here.

Although the ocean response presented here is for just one model and one SRES scenario, the pattern appears to be relatively robust across the ensemble of GCMS used in the IPCC AR4 [Meehl *et al.*, 2007]. It is also the case, that even if the balance of ice loss from the ice sheets changes within likely bounds, then the the areas experiencing the largest SLR due to TIM will remain the same. Thus, we conclude that TIM will be of critical importance to regional SLR in the Equatorial Pacific Ocean and, in particular, around Western Australia, Oceania and the small Atolls and islands in this region. We also conclude that SLR in the Arctic Ocean will be greater than the global mean and dominated by ocean processes with relatively little impact from TIM.

Acknowledgments. Work funded by the European Commission's 7$^{\text{th}}$ Framework Programme through grant number 226375 (ice2sea contribution number 104). We thank David Vaughan for helpful suggestions and encouragement. All figures have been drawn using GMT [Wessel and Smith, 1998].

References

Bamber, J. and R. Riva (2010), The sea level fingerprint of recent ice mass fluxes, *The Cryosphere*, *4*(4), 621–627.

Broeke, M., Bamber, J., Ettema, J., Rignot, E., Schrama, E., van de Berg, W.J., van Meijgaard, E., Velicogna, I. and Wouters, B. (2009), Partitioning Recent Greenland Mass Loss, *Science, 326*, 984–986.

Douglas, B. C. (1997), Global sea–level rise: a redetermination, *Surv. Geophys.*, *18*, 279–292.

Farrell, W. E. and J. A. Clark (1976), On postglacial sea–level, *Geophys. J. R. Astron. Soc., 46*, 647–667.

Fettweis, X. (2007), Reconstruction of the 1979–2006 Greenland ice sheet surface mass balance using the regional climate model MAR, *The Cryosphere*, *1*, 21–40.

Gardner, A. S., Moholdt, G., Wouters, B., Wolken, G. J., Burgess, D. O., Sharp, M. J., Cogley, J. G., Braun, C., and C. Labine (2011), Sharply increased mass loss from glaciers and ice caps in the Canadian Arctic Archipelago, *Nature, 473*, 357–360.

Giesen, R. H. and J. Oerlemans (2012), Global application of a surface mass balance model using gridded climate data, *The Cryosphere Discuss.*, *6*(2), 1445–1490.

Lenaerts, J. T. M., van den Broeke, M. R., van den Berg, W. J., van Meijgaard, E., and P. Kuipers Munneke (2012), A new, high-resolution, surface mass balance map of antarctica (1979-2010) based on regional atmospheric climate modeling, *Geophys. Res. Lett.*, L04501, 1-5, doi: 10.1029/2011GL050713.

McGranahan, G., Balk, D., and B. Anderson (2007), The rising tide: assessing the risk of climate change and human settlements in low elevation coastal zones, *Environment and Urbanization, 19,* 17–37.

Meehl, G. A., and 11 others (2007), Global Climate Projections, in Climate Change 2007: The Physical Science Basis. Contribution of Working Group I to the Fourth Assessment Report of the Intergovernmental Panel on Climate Change, edited by S. Solomon et al., Cambridge University Press, Cambridge.

Milne, G. A. and J. X.. Mitrovica (1998), Postglacial sea–level change on a rotating Earth, *Geophys. J. Int.*, *133*, 1–10.

Mitrovica, J. X., Tamiseia, M. E., Davis, J. L., and Milne, G. A. (2001). Recent mass balance of polar ice sheets inferred from patterns of global sea-level change. *Nature 409*, 1026–1029.

Moon, T., Joughin, I., Smith, B., and I. Howat (2012), 21st–century evolution of Greenland outlet glacier velocities, *Science*, *336*, 576–578.

Peltier W. R. (2004), Global glacial isostasy and the surface of the Ice–Age Earth: the ICE–5G(VM2) model and GRACE. *Annu. Rev. Earth Pl. Sc., 32*, 111–149.

Price, S. F., Payne, A. J., Howat, I. M., and Smith, B. E. (2011), Committed sea-level rise for the next century from Greenland ice sheet dynamics during the past decade, Proceedings of the National Academy of Sciences of the United States of America, 108, 8978–8983, 10.1073/pnas.1017313108, 2011.

Rignot, E., Bamber, J.L., van den Broeke, M.R., Davis, C., Li, Y., van de Berg, W.J. and Van Meijgaard, E. (2008), Recent Antarctic ice mass loss from radar interferometry and regional climate modelling, *Nat. Geosci., 1*, 106–110.

Rignot, E., Mouginot, J., and B. Scheuchl (2011a), Ice flow of the Antarctic ice sheet. *Science*, *333*, 1427–1430.

Rignot, E., Velicogna, I., van den Broeke, M., Monaghan, A. and J. Lenaerts (2011b), Acceleration of the contribution of the Greenland and Antarctic Ice Sheets to sea level rise, *Geophys. Res. Lett., 38*, L05503, 2011.

Riva, R. E. M., Bamber, J. L., Lavallee, D. A., and B. Wouters (2010), Sea–level fingerprint of continental water and ice mass change from GRACE, *Geophys. Res. Lett., 37*, L19605, doi:10.1029/2010GL044770.

Slangen, A.B.A., Katsman, C.A., van de Wal, R.S.W., Vermeersen, L.L.A. and R.E.M. Riva (2012), Towards regional projections of twenty–first century sea–level change based on IPCC SRES scenarios, *Clim. Dyn.,* doi:10.1007/s00382–011–1057–6.

Spada, G. and P. Stocchi (2007), SELEN: a Fortran 90 program for solving the "Sea Level Equation", *Comput. Geosci., 33* (4), 538–562. doi: 10.1016/j.cageo.2006.08.006.

Spada, G., Ruggieri, G., Sorensen, L. S., Nielsen, K., Melini, D., and F. Colleoni (2012), Greenland uplift and regional sea level changes from ICESat observations and GIA modelling, *Geophys. J. Int.*, *189* (3), 1457–1474.

Wessel, P. and W. H. F. Smith (1998), New, improved version of generic mapping tools released, *Eos Trans. AGU, 79,* 579.

Woodward, R. S. (1888). On the form and position of mean sea level, *United States Geological Survey Bulletin, 48*, 87–170.

Yin, J. J., Griffies, S. M. and R. J. Stouffer (2010), Spatial Variability of Sea Level Rise in Twenty-First Century Projections, *J. Clim., 23*(17), 4585–4607.

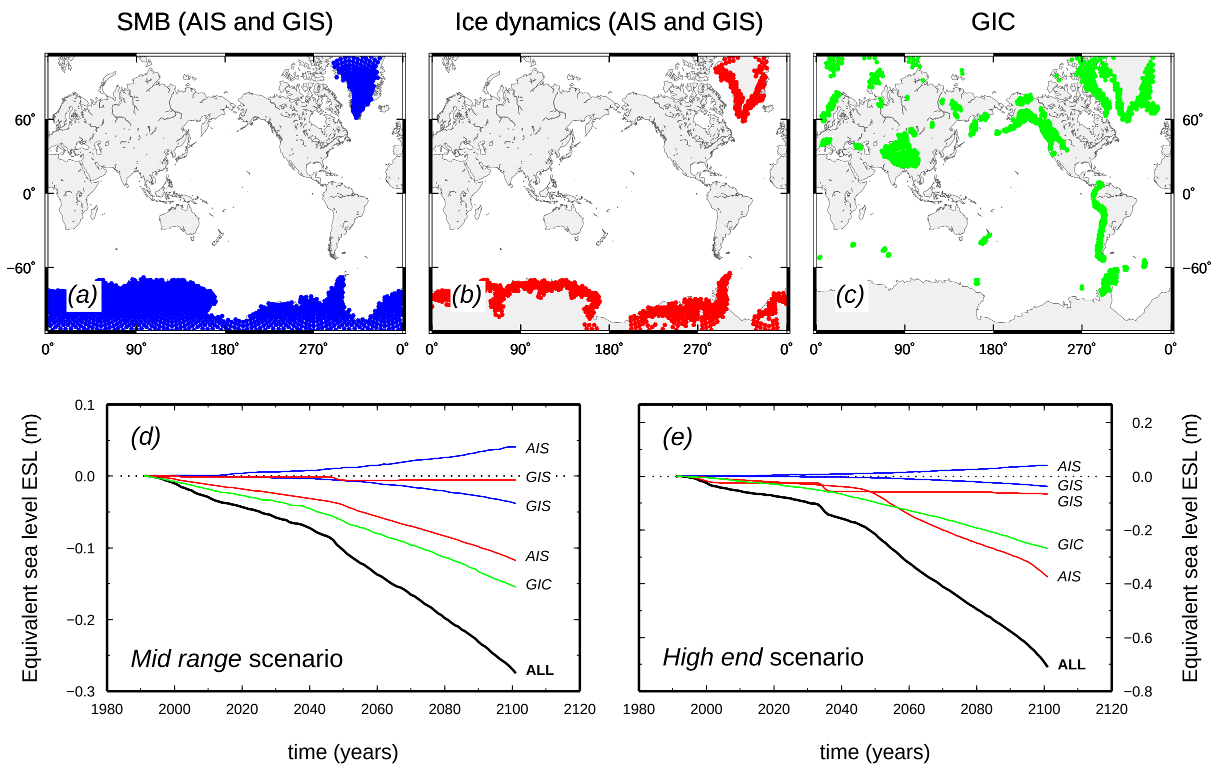

Figure 1. Top: spatial distributions of the ice sources used in this study: SMB (a), ice dynamics (b) and GICs (c). SMB and ice dynamics sources are further separated into AIS and GIS components. Bottom: time history of ESL (equivalent sea–level) since 1992, corresponding to the sources in (a–c), for the MR (d) and HE (e) scenarios, respectively. ALL curves show the total ESL variation.

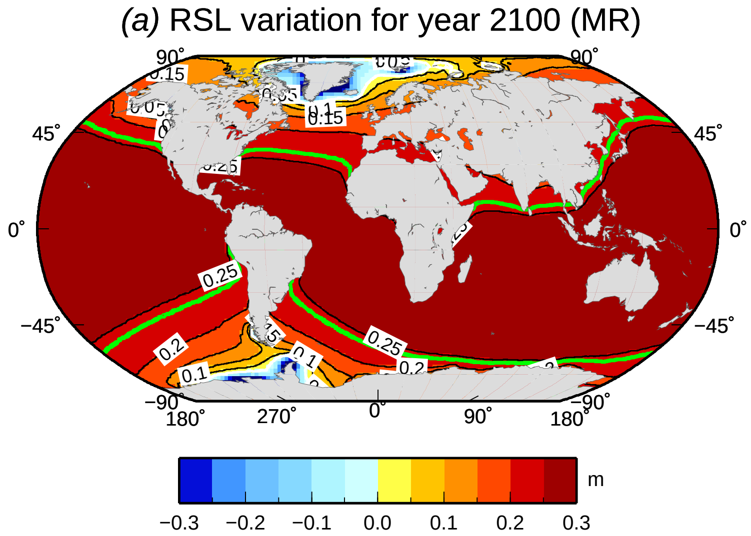

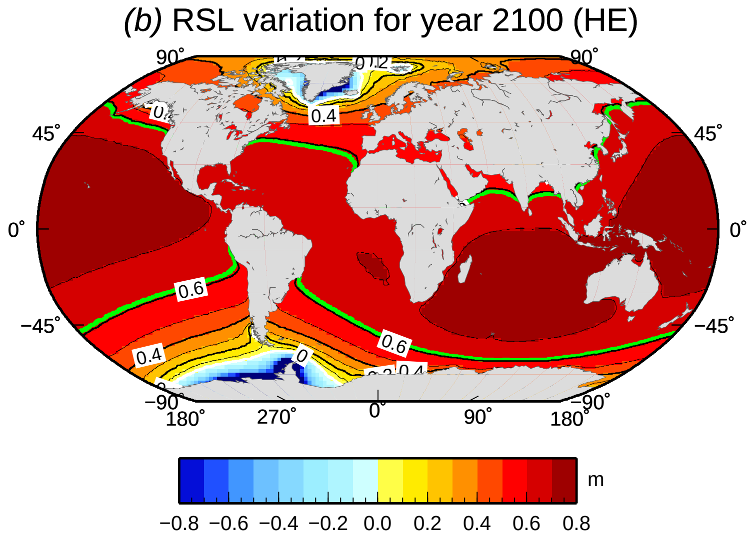

Figure 2. Fingerprint of the TIM RSL variation (m) for the year 2100 (relative to year 1992) pertaining to the MR (a) and HE scenarios (b). The green contour shows the ocean–averaged value (eustatic variation). The GIA component of sea–level change is not considered here.

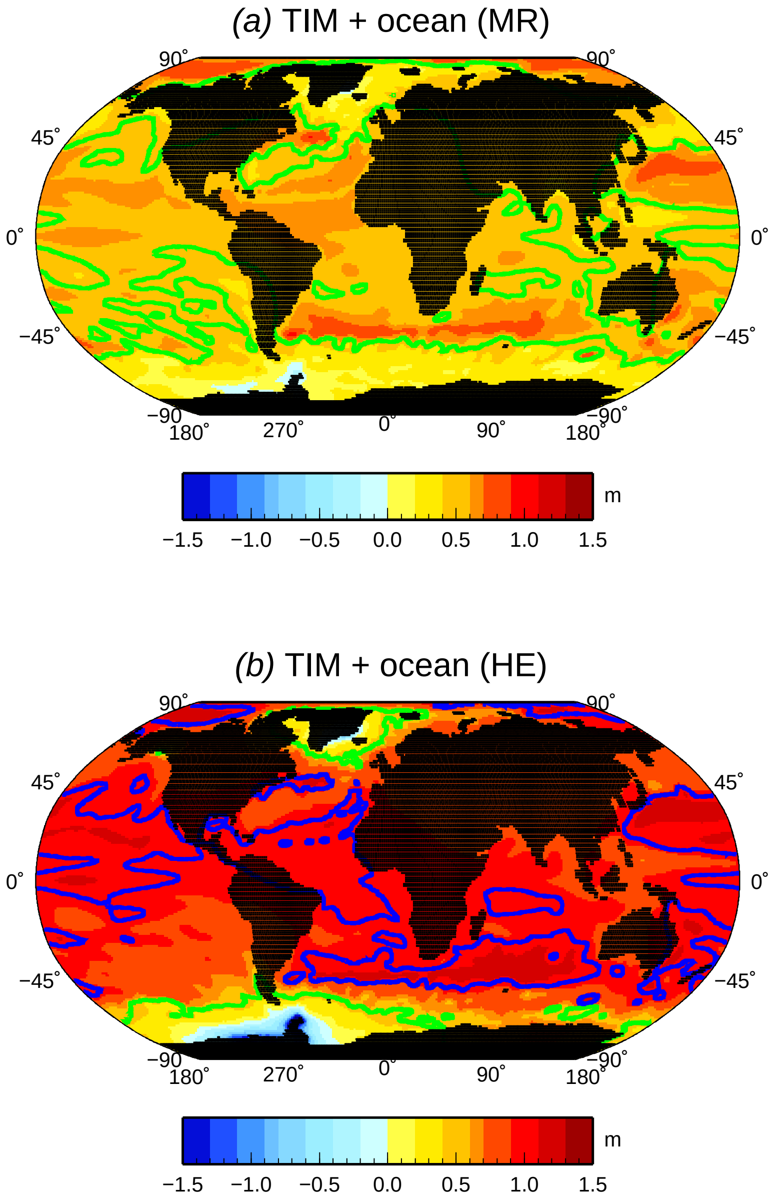

Figure 3. Total SLR (TIM plus ocean component) for the year 2100 and based on the MR (a) and HE scenarios (b), respectively. The green contour line corresponds to a SLR of 0.5 m; the blue one in (b) to a SLR of 1.0 m.

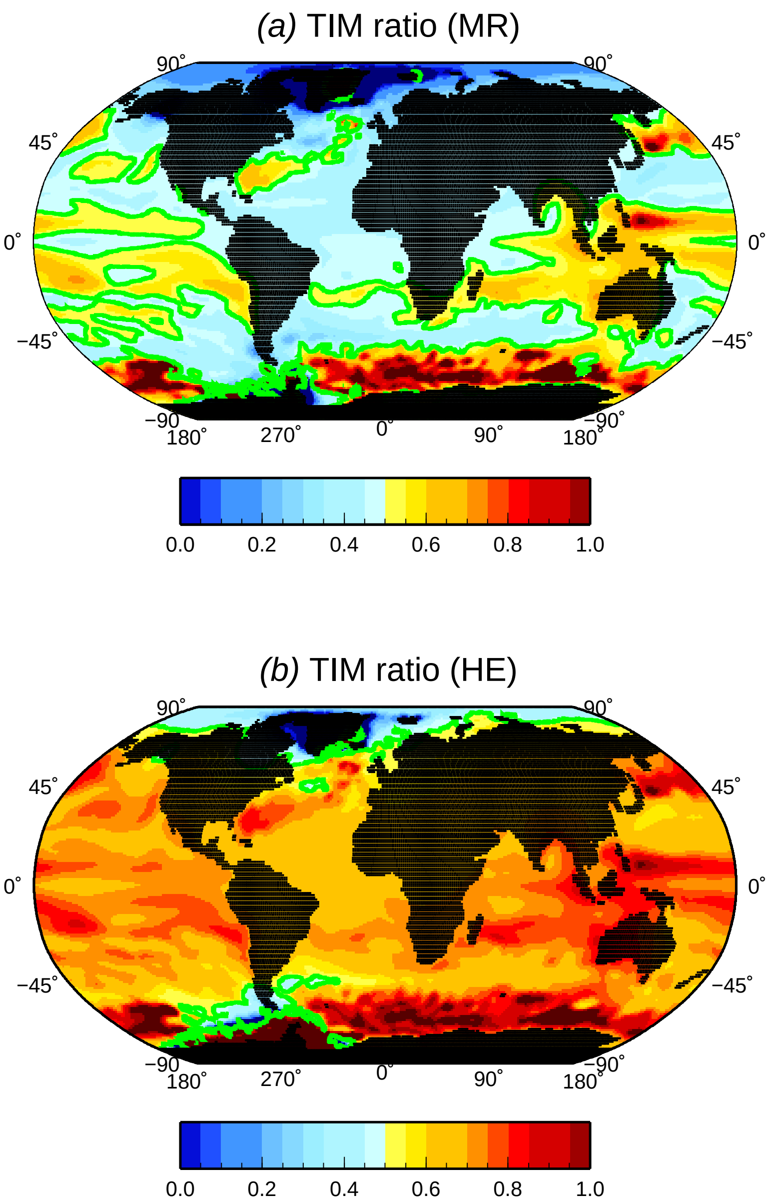

Figure 4. Ratio of the TIM component of total SLR expected for the year 2100 and based on the MR (top) and HE scenarios (bottom), respectively. The green contour line shows the a ratio of 0.5, where the contribution of TIM and ocean processes is equal.